

Vision Aided Environment Semantics Extraction and Its Application in mmWave Beam Selection

Feiyang Wen, Weihua Xu, Feifei Gao, Chengkang Pan, and Guangyi Liu

Abstract—In this letter, we propose a novel mmWave beam selection method based on the environment semantics that are extracted from camera images taken at the user side. Specifically, we first define the environment semantics as the spatial distribution of the scatterers that affect the wireless propagation channels and utilize the keypoint detection technique to extract them from the input images. Then, we design a deep neural network with environment semantics as the input that can output the optimal beam pairs at UE and BS. Compared with the existing beam selection approaches that directly use images as the input, the proposed semantic-based method can explicitly obtain the environmental features that account for the propagation of wireless signals, and thus reduce the burden of storage and computation. Simulation results show that the proposed method can precisely estimate the location of the scatterers and outperform the existing image or LIDAR based works.

Index Terms—Beam selection, mmWave, environment semantics, deep learning, computer vision

I. INTRODUCTION

MILLIMETER wave (mmWave) with beamforming is a critical technology for the next-generation wireless communications and is able to achieve a higher transmission rate. However, the traditional beamforming approaches, e.g., pilot based strategies [1] or beam sweeping [2], are bottlenecked by a high spectrum overhead, especially for time-varying scenarios such as vehicle-to-infrastructure (V2I) communications. Recently, it has been indicated that with the aid of the environment sensing information, such as point clouds [3]- [5] and images [6]- [9], one can implement beamforming with lower latency and less spectrum resources.

In [3], the authors utilize a deep neural network (DNN) classifier to predict the optimal beam pairs from the point clouds scanned by LIDAR. The authors of [4] and [5] optimize the LIDAR-based method with federated learning strategies and various deep learning techniques. With the aid of images taken at the base station (BS) side, [6] presents a multi-modal beam prediction scheme, and [9] proposes a strategy for proactive blockage prediction and user hand-off. Based on images from the camera view of mobile station (MS), the authors of [7] perform channel covariance matrix estimation, and the authors of [8] propose a beam alignment method aided by the object detection techniques.

F. Wen, W. Xu, and F. Gao are with Institute for Artificial Intelligence, Tsinghua University (THUAI), Beijing National Research Center for Information Science and Technology (BNRist), Department of Automation, Tsinghua University, Beijing, P.R. China, 100084 (email: wenfy20@mails.tsinghua.edu.cn, xwh19@mails.tsinghua.edu.cn, feifeigao@ieee.org).

C. Pan and G. Liu are with China Mobile Research Institute, Beijing, China. (e-mail: panchengkang@chinamobile.com; liuguangyi@chinamobile.com).

However, the existing vision based approaches are implemented in a straightforward manner, i.e. the optimal beam pairs are directly predicted from the input images, which may lead to certain disadvantages. According to the discrete physical model for wireless propagation [10], among all the environmental characteristics, only a few scatterers can significantly affect the wireless channel. Hence, there is vast amounts of redundancy in the images, which reduces the training efficiency, causes the overfitting, and declines the accuracy of the beam selection. Moreover, without explicitly extracting the effective scatterers, the existing methods have to use more complicated DNN models, leading to a huger computing and storage burden. To precisely represent the propagation environment, the semantic information of the images, i.e. the characteristics that account for the propagation of wireless signal, should be extracted. Hence, we define the *environment semantics* by considering the spatial distribution of the effective scatterers.

In this letter, we propose a vision aided environment semantics extraction method, and apply it in beam selection for V2I communication scenarios. In order to eliminate the redundant information, we represent the environment semantics as *semantic heatmaps*, and extract the heatmaps from the input images. Then, the optimal beam pair is predicted by another neural network from the heatmaps. Simulation results indicate that the proposed method can precisely capture the environment semantics, and outperform the existing image or LIDAR based methods.

II. SYSTEM MODEL

A. Channel Model

We consider a downlink V2I communication system, where a stationary BS is serving an MS on vehicle in mmWave band. Both BS and MS are equipped with a uniform planar array (UPA), and the numbers of antennas are $N_B = N_B^a \times N_B^b$ and $N_M = N_M^a \times N_M^b$, respectively. The channel matrix \mathbf{H} can be obtained by the widely-adopted geometric channel model:

$$\mathbf{H} = \sum_{p=1}^P \alpha_p \mathbf{a}_r(\theta_p^A, \varphi_p^A) \mathbf{a}_t^H(\theta_p^D, \varphi_p^D), \quad (1)$$

where P is the number of multipath components (MPC), α_p denotes the complex gain of the p th propagation path, and $\theta_p^A, \varphi_p^A, \theta_p^D, \varphi_p^D$ are the elevation and azimuth of the angle of arrival and departure of the p th path, respectively. Moreover,

the steering vectors $\mathbf{a}_r(\theta_p^A, \varphi_p^A) \in \mathbb{C}^{N_M \times 1}$, $\mathbf{a}_t(\theta_p^D, \varphi_p^D) \in \mathbb{C}^{N_B \times 1}$ are defined as

$$\mathbf{a}(N^a, N^b; \theta, \varphi) = \frac{1}{\sqrt{N^a N^b}} [1, \dots, e^{j\pi(a \cos \theta + b \sin \theta \sin \varphi)}, \dots, e^{j\pi((N^a-1) \cos \theta + (N^b-1) \sin \theta \sin \varphi)}]. \quad (2)$$

Then, we have $\mathbf{a}_r = \mathbf{a}(N_M^a, N_M^b)$ and $\mathbf{a}_t = \mathbf{a}(N_B^a, N_B^b)$.

Assume that BS and MS are equipped with fixed beam codebooks. For transmitter the codebook is $\mathcal{W}_B = \{\mathbf{w}_B^1, \mathbf{w}_B^2, \dots, \mathbf{w}_B^{C_B}\}$, while for receiver the codebook is $\mathcal{W}_M = \{\mathbf{w}_M^1, \mathbf{w}_M^2, \dots, \mathbf{w}_M^{C_M}\}$, where $\mathbf{w}_B^i \in \mathbb{C}^{N_B \times 1}$, $\mathbf{w}_M^j \in \mathbb{C}^{N_M \times 1}$ denote the transmitting and receiving vector. Under the noise-free assumption, the received power gain of beam pair $(\mathbf{w}_B^i, \mathbf{w}_M^j)$ is

$$y_{ij} = |(\mathbf{w}_M^j)^H \mathbf{H} \mathbf{w}_B^i|^2. \quad (3)$$

The goal is to select the optimal beam pair from the beam codebook that can maximize the power gain, i.e.

$$(\mathbf{w}_B^{i*}, \mathbf{w}_M^{j*}) = \arg \max_{\mathbf{w}_B^i \in \mathcal{W}_B, \mathbf{w}_M^j \in \mathcal{W}_M} y_{ij}. \quad (4)$$

B. Definition of the Semantic Heatmaps

To represent the environment semantics, we define the effective scatterers, and generate the semantic heatmaps by projecting the effective scatterers into the camera view of MS.

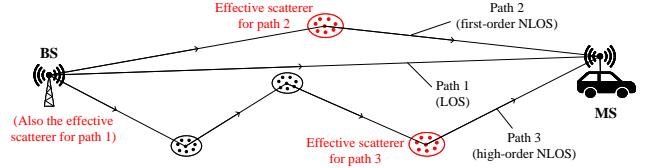
Note that the weak paths have less impact on the channel, and taking them into consideration would increase the computing and storage burden. Therefore, we neglect the paths with $|\alpha_p|^2 / |\alpha_{max}|^2 < P_{th}$, where $|\alpha_{max}|^2$ denotes the power gain of the strongest path in a scene, and P_{th} is a tuneable threshold to trade off the accuracy against the computing resource consumption. As shown in Fig. 1(a), for each NLOS path, we define the scatterer that reflects the last hop along the signal propagation as the *effective scatterer*; while for the LOS path, BS can serve as the effective scatterer. In this way, we ensure that all the effective scatterers are in the camera view of MS, and can be then extracted from the images.

We assume that MS is equipped with N_C monocular cameras, which are installed at different azimuths to provide multi-view images. Meanwhile, all the cameras are equipped at the same place with the antenna.¹ We define the elevation and the azimuth of the i th camera relative to MS as $(\theta_i^C, \varphi_i^C)$, the size of taken image as $H^C \times W^C$, and the camera's horizontal field of view as $2\beta_i$. If the p th effective scatterer is in the i th camera's field of view, then it is projected onto the coordinate (x_p^C, y_p^C) of the image plane as

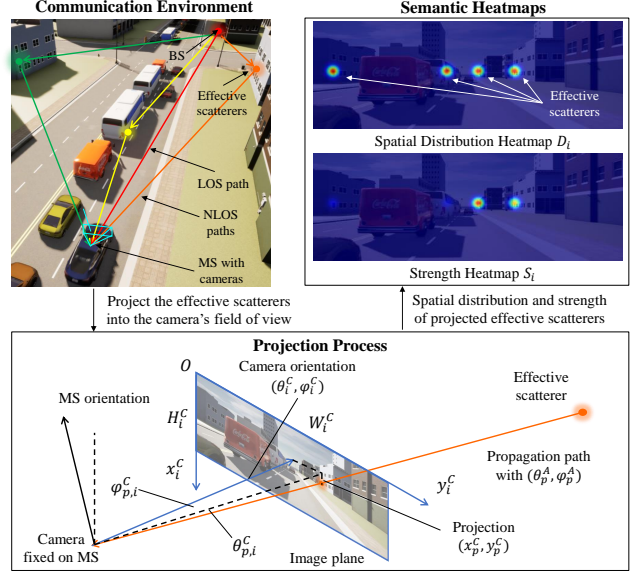
$$\begin{bmatrix} x_p^C \\ y_p^C \\ 1 \end{bmatrix} = \begin{bmatrix} \frac{W^C}{2 \tan \beta_i} & 0 & H^C/2 \\ 0 & \frac{W^C}{2 \tan \beta_i} & W^C/2 \\ 0 & 0 & 1 \end{bmatrix} \begin{bmatrix} \frac{\tan \theta_{p,i}^C}{\cos \varphi_{p,i}^C} \\ \tan \varphi_{p,i}^C \\ 1 \end{bmatrix}, \quad (5)$$

where $\theta_{p,i}^C = \theta_p^A - \theta_i^C$ and $\varphi_{p,i}^C = \varphi_p^A - \varphi_i^C$ denote the elevation and the azimuth of the p th path in the i th camera's field of view.

¹In practice, if the cameras are fixed far away from the antenna, then one can utilize novel view synthesis techniques [16] to generate the antenna-view images from other camera views.



(a) The definition of effective scatterers.



(b) The generation of semantic heatmaps.

Fig. 1. An illustration to the semantic heatmaps.

Based on the projection process, we generate two types of heatmaps for each camera view: the spatial distribution heatmap D_i and the strength heatmap S_i . Both the heatmaps are coincident with the image plane at a lower resolution, i.e. $D_i, S_i \in [0, 1]^{\frac{H^C}{R} \times \frac{W^C}{R}}$, and the p th scatterer's coordinate is denoted as $(x_p^H, y_p^H) = (\lfloor \frac{x_p^C}{R} \rfloor, \lfloor \frac{y_p^C}{R} \rfloor)$. The corresponding elements of the heatmaps are set to $D_i(x_p^H, y_p^H) = 1$ and $S_i(x_p^H, y_p^H) = |\alpha_p|^2 / |\alpha_{max}|^2$, respectively. Then, as a measure to improve the prediction performance of DNN, we splat all projected points on D_i and S_i using a Gauss kernel $K = \exp(-\frac{(x-x_{p,i}^H)^2 + (y-y_{p,i}^H)^2}{2\sigma^2})$ [14], where σ is an empirical parameters decided by the size of heatmaps.

III. VISION BASED ENVIRONMENT SEMANTIC EXTRACTION AND BEAM SELECTION

To obtain the optimal beam pairs in (4), we propose a two-stage beam selection approach, as shown in Fig. 2. We assume that the location and the orientation of MS can be obtained by vehicular sensors like inertial measuring units and GPS receivers, and the location of BS is known. Therefore, the location (x_M, y_M, z_M) and the orientation θ_M of MS relative to BS is available.

Different from [6], [9], during the communication process, the optimal beam pairs are predicted by MS. In the first stage, MS obtains its location information and multi-view images, and send them to a well-designed DNN to extract the semantic heatmaps. In the second stage, based on the semantic heatmaps and the location information, another DNN will be designed

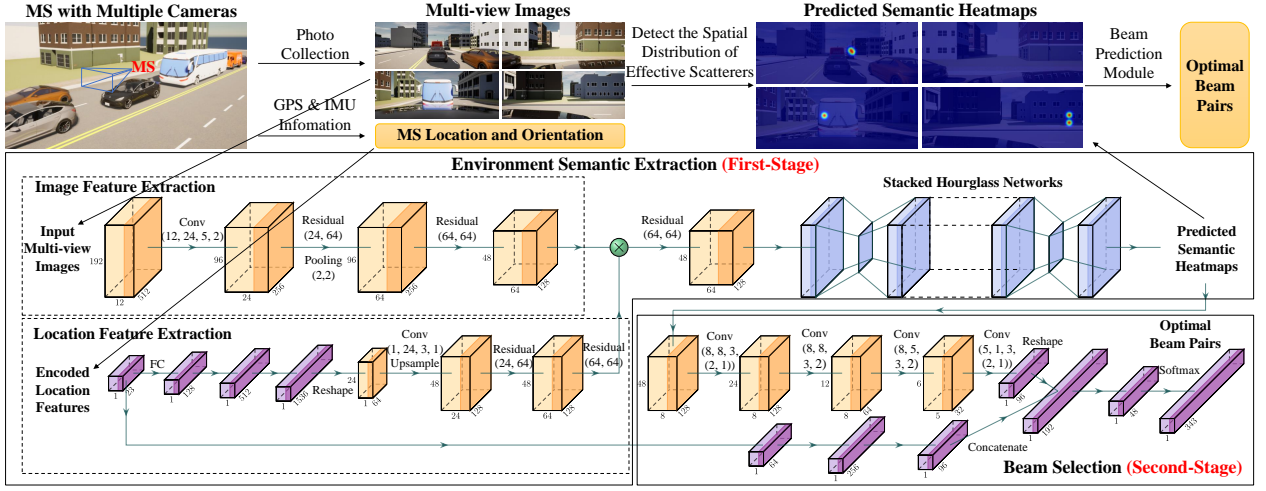


Fig. 2. The proposed deep learning based method for environment semantics extraction and beam selection.

to predict the optimal beam pairs and feed them back to BS. In the following sections, we will present the two stages in detail.

A. Environment Semantics Extraction

1) *Preprocessing*: At each time step, MS obtains multiple RGB images I_1, I_2, \dots, I_{N_C} , where $I_i \in \mathbb{R}^{H^C \times W^C \times 3}$, and the location information that satisfies $(x_M, y_M, z_M, \theta_M) \in \mathbb{R}^4$. We simply concatenate the images in the channel dimension to obtain the input image feature $I_{in} \in \mathbb{R}^{H^C \times W^C \times 3N_C}$. However, as shown in [15], a DNN can poorly represent high-frequency features from the raw coordinate form of the location information, leading to a limited performance. Hence, we encode x_M, y_M using a high-frequency function [15]:

$$\gamma(p) = (\sin(2^0 \pi p), \cos(2^0 \pi p), \dots, \sin(2^{L-1} \pi p), \cos(2^{L-1} \pi p)), \quad (6)$$

where L is set to 5. The input location vector is concatenated as $L_{in} = (\gamma(x_M), \gamma(y_M), z_M, \cos \theta_M, \sin \theta_M) \in \mathbb{R}^{23}$.

2) *Semantic Extraction via Keypoint Detection*: The semantic extraction network takes I_{in}, L_{in} as input, and predicts the semantic heatmap $\hat{H} \in [0, 1]^{\frac{H^C}{R} \times \frac{W^C}{R} \times 2N_C}$, where the first N_C channels and the last N_C channels correspond to D_i and S_i for each camera view, respectively.

As shown in Fig. 2, we use a convolutional layer and several residual blocks [17] to extract the image feature map from I_{in} . Meanwhile, we use fully connected layers, 2-D reshape layer, and residual blocks to obtain the location feature map from L_{in} . The image feature map can represent the interplay of environment scatterers, especially for the dynamic scatterers like vehicles, while the location feature map contains the exact geometric relation between BS and MS. We fuse the two feature maps with the operation of multiplication in order to fully exploit the contained information. Next, we adopt the stacked hourglass networks [11], [12] to predict \hat{H} . Generally, the hourglass networks capture multi-scale spatial relationships through repeated compressing-upsampling architecture.

We use a variation of focal loss [13], [14] L_D

$$L_D = - \sum_{x,y;C=1}^{N_C} \begin{cases} (1 - \hat{H}_{xyC})^2 \log(\hat{H}_{xyC}), & \text{if } H_{xyC} = 1 \\ (1 - H_{xyC})^4 \hat{H}_{xyC}^2 \log(1 - \hat{H}_{xyC}), & \text{otherwise} \end{cases} \quad (7)$$

for D_i and MSE loss $L_S = \sum_{x,y;C=N_C+1}^{2N_C} (\hat{H}_{xyC} - H_{xyC})^2$ for S_i , respectively, where H is the groundtruth of \hat{H} . The heatmap prediction loss is defined as $L_{hm} = L_D + L_S$.¹

B. Beam Selection

The beam selection network takes the predicted semantic heatmap \hat{H} and location vector L_{in} as inputs. We process \hat{H} by several convolutional layers, and process L_{in} via fully connected layers. Next, two fully connected layers followed by a softmax layer are adopted to yield the prediction vector $\hat{y}_{ij} \in [0, 1]^{N_B \times N_M}$. The predicted optimal beam pair is then $(\hat{i}, \hat{j}) = \arg \max_{i,j} y_{ij}$.

The loss function for beam prediction is defined as [5]

$$L_{pd} = -(1 - \beta) \sum_{i,j} y_{ij}^* \log(\hat{y}_{ij}) - \beta \sum_{i,j} \bar{y}_{ij} \log(\hat{y}_{ij}), \quad (8)$$

where \bar{y}_{ij} is the normalized form of power gain y_{ij} ; $y_{ij}^* = 1$ for (i^*, j^*) and $y_{ij}^* = 0$ on other components; $\beta \in [0, 1]$ is a tuneable hyperparameter. The overall loss function is then defined as $L_{all} = L_{pd} + L_{hm}$.

IV. SIMULATION RESULTS

A. Simulation Setup

As shown in Fig. 3, we delineate a rectangle with width W_A and length L_A as the coverage area of BS in the autonomous driving simulation software CARLA [18]. Then, we utilize the traffic simulation software SUMO [19] to generate a continuous traffic flow, which contains 5 types of vehicles as listed in TABLE I. The vehicles move according to the routes and velocities planned by SUMO, and the locations of

¹During the training phase, AOAs and power gains of the major propagation paths are required to generate H . In practice, they can be obtained via channel estimation or AOA estimation algorithms.

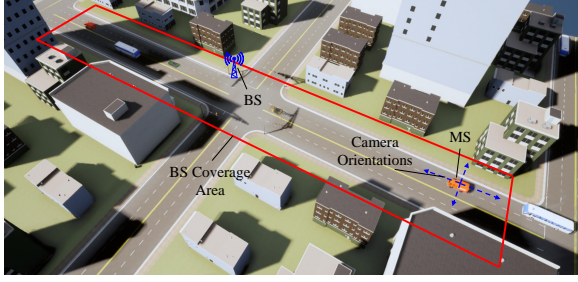


Fig. 3. The simulation scenario in CARLA.

TABLE I
SIMULATED VEHICLE TYPES

Type	Car#1	Car#2	Car#3	Van	Bus
Length/m	4.81	4.90	4.15	5.20	11.08
Width/m	2.17	2.06	2.00	2.62	3.25
Height/m	1.52	1.48	1.38	2.48	3.33

TABLE II
RAY TRACING PARAMETERS FOR WIRELESS INSITE

Parameter	Value
Carrier Frequency	60GHz
Propagation Model	X3D
Building Material	Concrete
Vehicle Material	Metal
Maximum Number of Reflections	6
Maximum Number of Diffractions	1
Maximum Paths Per Receiver Point	25

vehicles are synchronized to CARLA. Once a vehicle moves in the coverage area of BS, the cameras on the vehicle will take images at a regular time interval T_C . Meanwhile, the entire simulation scene will be recorded and synchronized to the ray tracing software Wireless Insite [20] for wireless channel simulation, in which all the vehicles are converted into cubes with the same sizes, positions, and orientations as those in CARLA. In this way, we generate the dataset containing MS locations, images and corresponding channel information.

We set $W_A = 48\text{m}$, $L_A = 192\text{m}$ and $T_C = 0.5\text{s}$; the UPA of BS is fixed at 3m above the street, and the UPA of MS is fixed at 0.1m above the roof center of the vehicle; the cameras are installed horizontally with $N_C = 4$, $\varphi_i^C = 0^\circ, 90^\circ, 180^\circ, 270^\circ$ respectively, $2\beta_i = 90^\circ$, and $H_C \times W_C = 192 \times 512$ in pixels. For semantic heatmaps, we set $\frac{H_C}{R} \times \frac{W_C}{R} = 48 \times 128$, $P_{th} = -10\text{dB}$, and $\sigma = 1.5$. The ray tracing parameters are shown in TABLE II; $N_B^a = N_M^a = 8$, $N_B^b = N_M^b = 64$, $C_B = C_M = 64$; $\mathbf{w}_B^i = \mathbf{a}_t(\theta_t, \frac{2i-C_B-1}{2C_B}\pi)$, $i = 1, 2, \dots, C_B$ and $\mathbf{w}_M^j = \mathbf{a}_r(\theta_r, \frac{2j-C_M-1}{2C_M}\pi)$, $i = 1, 2, \dots, C_M$, where $\theta_t = 92^\circ$ and $\theta_r = 88^\circ$ according to the heights of BS and MS. We choose 343 candidate beam pairs, which have become optimal for more than three times in the whole dataset. In total, we obtain 24892 channel samples in 2000 simulation scenes. The training set contains 13123 LOS samples and 4761 NLOS samples, while the testing set contains 3765 LOS samples and 3243 NLOS samples.

The number of channels, layers, and stacks of the hourglass networks are 64, 4, and 2 respectively; β is set to 0.8. We

TABLE III
PERFORMANCE COMPARISON BETWEEN DIFFERENT METHODS

Model	Proposed	LIDAR	VBALA
A(1)	60.77%	45.96%	47.56%
T(1)	82.15%	68.37%	71.40%
A(5)	77.94%	71.35%	73.09%
T(5)	91.44%	87.17%	88.55%

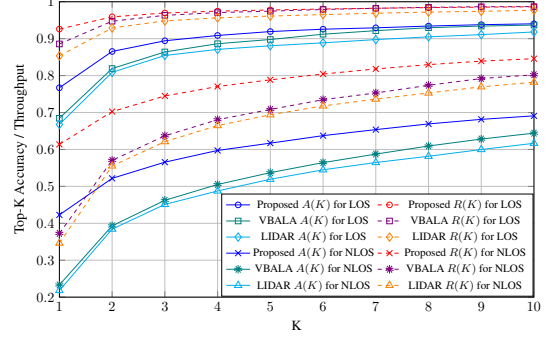


Fig. 4. Top-K beam selection accuracy and throughput ratio of the three methods for LOS and NLOS testing samples.

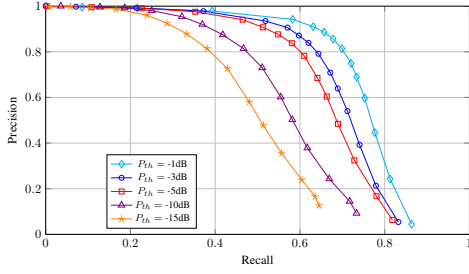
utilize batch normalization for each convolutional layer or residual block. The details are presented in Fig. 2.

B. Numerical Results

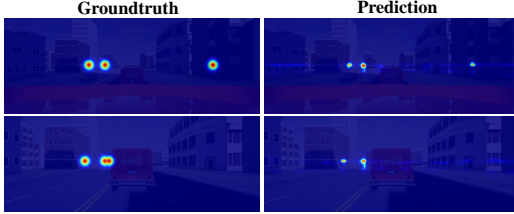
We compare the proposed beam selection algorithm with LIDAR-based method [5] and vision based method VBALA [8]. The LIDAR-based method uses DNN to perform beam selection from the point cloud, while VBALA predicts the optimal beam pairs from the vehicle distribution information captured by 3D object detection. For the LIDAR-based method, we equip each MS with a LIDAR at 1m above the roof center of the vehicle, which has a coverage radius of 100m. For VBALA, we set the grid size $L_G = 12\text{m}$ and $W_G = 2\text{m}$. For fairness, all three methods are trained for 30 epochs, using the same beam prediction loss function L_{pd} in (8).

Similar to [5], we evaluate the top-K accuracy $A(K)$ with the throughput ratio $T(K)$. As shown in Fig. 4 and TABLE III, The top-1 accuracy and throughput ratio of the proposed method reach 60.77% and 82.15%, which outperform VBALA by 13% and 11%, respectively. Meanwhile, we compare the three methods for LOS and NLOS testing samples. Though the proposed method can outperform baseline methods in LOS cases, its major advantage is exhibited in NLOS cases, where the accuracy is approximately 20% higher than VBALA for top-1, and 9% higher in average. Since the environment semantics can be extracted in an explicit manner, the proposed method has a deeper perception of multipath effects and blockages, leading to a better NLOS performance.

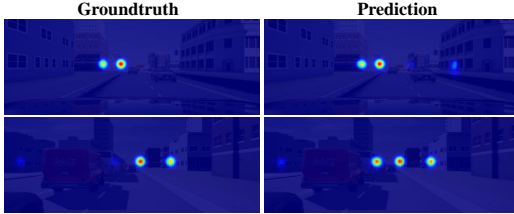
Moreover, we note that the threshold P_{th} can affect the accuracy and the storage overhead of the proposed method. Specifically, we define the averaged number of effective scatterers per camera view as N_E , which reflects the storage requirement of the training dataset. As shown in TABLE IV, the proposed method achieves the highest accuracy at $P_{th} = -10\text{dB}$. Moreover, when $P_{th} < -5\text{dB}$, the consumption of



(a) The precision-recall curves. The distance threshold is 3 pixels, which corresponds to an angular misalignment of approximately 2.1° .



(b) Visualization of spatial distribution heatmaps.



(c) Visualization of strength heatmaps.

Fig. 5. The performance of semantic extraction. Assuming the number of groundtruth, predicted, and successfully detected scatterers are N_g, N_p, N_d , the precision and the recall are defined as N_d/N_p and N_d/N_g respectively.

TABLE IV
PERFORMANCE COMPARISON BETWEEN DIFFERENT THRESHOLDS

P_{th}	-1dB	-3dB	-5dB	-10dB	-15dB
A(1)	58.92%	59.18%	59.63%	60.77%	59.91%
T(1)	80.83%	80.99%	81.31%	82.15%	82.10%
A(5)	76.56%	76.78%	77.05%	77.94%	77.50%
T(5)	90.82%	90.77%	90.99%	91.44%	91.22%
N_E	0.322	0.406	0.483	0.786	1.227

storage resources will be significantly reduced without a major decrease in accuracy.

Furthermore, we evaluate the effectiveness of the environment semantics extraction in Fig. 5. We obtain the maximum points on predicted spatial distribution heatmaps by non-maximum suppression. If the distance between the predicted maximum point and the groundtruth is within a threshold, then the corresponding scatterer will be perceived to be detected. Besides, since the stronger paths can more significantly influence the channel, the corresponding scatterers should be extracted more precisely. Therefore, we adjust the threshold P_{th} , train the corresponding semantics extraction model, and evaluate the precision-recall curves as shown in Fig. 5(a). It can be seen that the proposed method successfully extracts the effective scatterers from input images, especially for the stronger ones.

V. CONCLUSION

We have proposed a vision aided environment semantic extraction method, and apply it in mmWave beam selection. We define the environment semantics as the spatial distribution of effective scatterers, which are represented as the semantic heatmaps, and we extract them via keypoint detection techniques. Compared with the existing image or LIDAR based methods, the proposed method shows deeper insight into the wireless propagation environment. Simulation results indicate that the proposed method can significantly outperform the existing methods in accuracy, and lead to a lower overhead for beam selection.

REFERENCES

- [1] V. Venkateswaran and A.-J. van der Veen, "Analog beamforming in MIMO communications with phase shift networks and online channel estimation," *IEEE Trans. Signal Process.*, vol. 58, no. 8, pp. 4131-4143, Aug. 2010.
- [2] J. Song, J. Choi, and D. J. Love, "Common codebook millimeter wave beam design: Designing beams for both sounding and communication with uniform planar arrays," *IEEE Trans. Commun.*, vol. 65, no. 4, pp. 1859-1872, Apr. 2017.
- [3] A. Klautau, N. González-Prelcic, and R. W. Heath, "LIDAR data for deep learning-based mmWave beam-selection," *IEEE Wireless Commun. Lett.*, vol. 8, no. 3, pp. 909-912, Jun. 2019.
- [4] M. B. Mashhadi, M. Jankowski, T.-Y. Tung, S. Kobus, and D. Gündüz, "Federated mmWave beam selection utilizing LIDAR data," *IEEE Wireless Commun. Lett.*, vol. 10, no. 10, pp. 2269-2273, Oct. 2021.
- [5] M. Zecchin, M. B. Mashhadi, M. Jankowski, D. Gündüz, M. Kountouris, and D. Gesbert, "LIDAR and position-aided mmWave beam selection with non-local CNNs and curriculum training," *IEEE Trans. Veh. Technol.*, vol. 71, no. 3, pp. 2979-2990, Mar. 2022.
- [6] G. Charan, T. Osman, A. Hredzak, N. Thawdar, and A. Alkhateeb, "Vision-position multi-modal beam prediction using real millimeter wave datasets," *2022 IEEE Wireless Commun. Netw. Conf. (WCNC)*, 2022, pp. 2727-2731.
- [7] W. Xu, F. Gao, J. Zhang, X. Tao, and A. Alkhateeb, "Deep learning based channel covariance matrix estimation with user location and scene images," *IEEE Trans. Commun.*, vol. 69, no. 12, pp. 8145-8158, Dec. 2021.
- [8] W. Xu, F. Gao, X. Tao, J. Zhang, and A. Alkhateeb, "Computer vision aided mmWave beam alignment in V2X communications," *IEEE Trans. Wireless Commun.*, 2022.
- [9] G. Charan, M. Alrabeiah, and A. Alkhateeb, "Vision-aided 6G wireless communications: Blockage prediction and proactive handoff," *IEEE Trans. Veh. Technol.*, vol. 70, no. 10, pp. 10193-10208, Oct. 2021.
- [10] A. M. Sayeed, "Deconstructing multiantenna fading channels," *IEEE Trans. Signal Process.*, vol. 50, no. 10, pp. 2563-2579, Oct. 2002.
- [11] A. Newell, K. Yang, and J. Deng, "Stacked hourglass networks for human pose estimation," in *Proc. Eur. Conf. Comput. Vis. (ECCV)*, 2016, pp. 483-499.
- [12] A. Newell, Z. Huang, and J. Deng, "Associative embedding: End-to-end learning for joint detection and grouping," in *Proc. Adv. Neural Inf. Process. Syst.*, 2017, pp. 2274-2284.
- [13] H. Law and J. Deng, "CornerNet: Detecting objects as paired keypoints," in *Proc. Eur. Conf. Comput. Vis. (ECCV)*, Sep. 2018, pp. 734-750.
- [14] K. Duan, S. Bai, L. Xie, H. Qi, Q. Huang, and Q. Tian, "CenterNet: Keypoint triplets for object detection," in *Proc. IEEE/CVF Int. Conf. Comput. Vis. (ICCV)*, Oct. 2019, pp. 6569-6578.
- [15] B. Mildenhall, P. P. Srinivasan, M. Tancik, J. T. Barron, R. Ramamoorthi, and R. Ng, "NERF: Representing scenes as neural radiance fields for view synthesis," in *Proc. Eur. Conf. Comput. Vis. (ECCV)*, 2020, pp. 405-421.
- [16] R. Tucker and N. Snavely, "Single-View view synthesis with multi-plane images," in *Proc. IEEE/CVF Conf. Comput. Vis. Pattern Recognit. (CVPR)*, 2020, pp. 548-557.
- [17] K. He, X. Zhang, S. Ren, and J. Sun, "Deep residual learning for image recognition," in *Proc. IEEE Conf. Comput. Vis. Pattern Recognit. (CVPR)*, 2016, pp. 770-778.
- [18] <https://carla.org>
- [19] <https://www.eclipse.org/sumo>
- [20] <https://www.remcom.com/wireless-insite-em-propagation-software>